Nonlinear Dynamics and Bifurcation Structure of a Stage-Structured Theta-Ricker Map with Cross-Stage Feedback

HAFIDH KHOERUL FATA *, NURCAHYA YULIAN ASHAR
Department of Mathematics, Faculty of Science and Mathematics
Universitas Diponegoro
Jl. Prof. Jacub Rais, Semarang, 50275
INDONESIA
**Corresponding Author*

Abstract: This study surveyed the nonlinear dynamics of a discrete-time, stage-structured population model merging demographic memory through adult survival. The model develops the classical θ–Ricker formulation by introducing cross-stage feedback between juvenile and adult compartments governed by a set of biologically interpretable parameters. The analytical results show that the system admits a unique positive equilibrium, the local stability of which is determined by the trace and determinant of the Jacobian matrix. Loss of stability occurs via two primary mechanisms: flip (period doubling) and Neimark–Sacker bifurcations. Explicit conditions for both bifurcations are derived, and the first Lyapunov coefficient is computed to characterize the direction and criticality of the Neimark–Sacker (NS) transition. Numerical experiments, including one-parameter bifurcation diagrams and two-parameter Lyapunov maps, confirmed the analytical predictions. Increasing the reproductive rate or cross-stage feedback leads to successive period doubling and chaos, whereas higher maturation efficiency and adult survival expand the stability domain. The results revealed that demographic memory acts as an internal damping mechanism that delays the onset of instability and suppresses chaotic oscillations. Overall, this study provides a coherent analytical–numerical framework for understanding how feedback and memory interact to shape complex population dynamics in stage-structured ecological systems.

Key-Words: Stage-structured population model, θ–Ricker map, cross-stage feedback, demographic memory, flip bifurcation, Neimark–Sacker bifurcation

Received: March 14, 2025. Revised: July 17, 2025. Accepted: August 9, 2025. Published: January 9, 2026.

1 Introduction

The discrete population model remains crucial in theoretical ecology because, despite its simplicity, it can produce period folding, quasiperiodicity, and chaos through density regulation. The Ricker map is a canonical example of the impact of feedback on long-term dynamics, [1]. Stage or delay structures capture demographic memory; intergenerational survival memory can alter stability and the domain of attraction, [2]. Small changes in reproductive feedback or cross-stage coupling can shift stable equilibria into oscillations or chaos, [3], [4], [5], [6]. For a general mathematical background on difference equations and discrete-time dynamical systems, see [7].

Gradual population research shows that density regulation cannot be explained by a single age class or a single nonlinearity; the Ricker and Hassell models, [8], ignore differences in survival between stages. Recent studies have shown that the presence of a stage structure and memory effects can fundamentally alter the dynamics of a system, [9]. El-Morshedy and Ruiz-Herrera showed that the addition of delayed feedback to stage-structured models can induce long-term oscillations even outside the local stability domain [2]. Mo and Shao confirm that delayed maturation narrows the stability region and triggers periodic bifurcations [10], while Liu, Guo, and Liu investigate rich bifurcation patterns in a stage-structured discrete model incorporating a birth-pulse mechanism [11]. Complementary perspectives on stability and bifurcation mechanisms in delay-influenced dynamical formulations are also discussed in [12].

Similar trends have been observed in predator–prey systems and exploitation models. Liz and Sovrano examined the hydra effect in stage-structured models and found that cross-stage regulation can produce unexpected bifurcations and oscillations, [13]. Khan and Uddin report period–doubling cascades and chaos in a discretized Holling-II model with Allee effects, [3], while Sharma et al. describe two-dimensional bifurcations in a discrete predator–prey model, [14]. In an evolutionary context, Mokni and Ch–Chaoui introduced a Darwinian Ricker–Cushing map

exhibiting Hopf transitions, [4]. Another study by El-Metwally et al. extended the Ricker map to a general form with an exponent θ controlling the density strength and revealed fundamental changes in asymptotic dynamics, [1].

The latest literature highlights the integration of three mechanisms: stage structure, memory effects, and nonlinear density regulation. However, most studies still separate them, so this gap forms the conceptual basis of the developed model. Bifurcation analysis in two-dimensional discrete systems remains important because it explains the transition from stable to oscillatory, quasiperiodic, and chaotic behavior. May showed that simple models can trigger folding cascades, [8]. Further studies on staged systems confirm their sensitivity: Liz and Sovrano discovered flip bifurcations and the *hydra* effect at harvest thresholds, [13]; Sharma et al. revealed a codimensional bifurcation linking flip and Neimark–Sacker thresholds, [14]; Khan and Uddin reported a recurrent cascade of chaos from the interaction of the Allee effect and prey protection, [3].

Other studies have indicated that stage structures can enrich bifurcation scenarios. Mokni and Ch–Chaoui report that Ricker–Cushing Darwinian dynamics exhibit Hopf transitions that serve as precursors to quasiperiodicity, [4], while El-Metwally et al. found that variations in density exponents in the general Ricker map can significantly shift the position of bifurcation curves, [1]. Recent research has highlighted the link between bifurcations and population control. Mo and Shao demonstrated that delaying predator–prey interactions produces quasiperiodic orbits that can be controlled via the delay parameter, [10]. Furthermore, Al–Kaff et al. demonstrated that a two-logistic-map-based prey–predator system exhibits Neimark–Sacker's characteristic Arnold tongues and complex chaos windows, [15].

The literature confirms that bifurcation phenomena in discrete ecological models are not merely the result of increased reproductive parameters but also of cross-stage interactions and nonlinear feedback. However, although various studies have examined one or two of these mechanisms, there have not been many approaches that explicitly combine the effects of stage structure, adaptive density exponents, and demographic memory in a single consistent analytical formulation. This gap is the main motivation for the local and global bifurcation analyses of the model proposed in this study.

Although previous studies have enriched our understanding of discrete population dynamics through stability and bifurcation analyses, existing approaches generally focus on only one or two regulatory mechanisms at a time. Stage-structured models are often described without considering inter-generational memory effects, whereas studies on delayed feedback rarely explicitly include cross-stage interactions. In contrast, extensions of the Ricker map with adaptive density exponents have generally been studied in single-dimensional systems, failing to represent the real ecological complexity involving differences in vital rates between individual classes.

This gap is the starting point of this study. We propose a two-stage model formulation that simultaneously integrates three main mechanisms: (i) a stage structure that distinguishes between young and adult individuals, (ii) memory effects through delayed feedback that influence population recruitment, and (iii) adaptive density exponents that control the intensity of the nonlinear regulation. The analysis focuses on characterizing fixed points, local stability, and the emergence of flip and Neimark–Sacker bifurcations as pathways to oscillations and quasiperiodicity. This approach extends the discrete population model theory and reveals how demographic memory and stage interactions trigger or dampen two-dimensional chaos.

2 Model Formulation and Preliminary Properties

This section formulates a two-dimensional map for a stage-structured population with θ-Ricker density regulation, as a biologically meaningful and mathematically defined model. This formulation combines two compartments, namely juvenile and adult, and incorporates memory effects through the survival of adults across generations. This model recovers the classic Hassell map as a special case when the memory parameter and density exponent take specific values. After introducing the mathematical form of the system, we examine its basic properties, including positivity, boundedness of orbits, and conditions for the existence and uniqueness of equilibria. These preliminary results also confirm the closedness of the dynamics on positive orbits, providing a solid foundation for the stability and bifurcation analysis in the next section.

2.1 Model Definition and Biological Interpretation

The model studied is a two-dimensional map that describes population dynamics with two age classes, juveniles (J_t) and adults (A_t), at discrete times $t \in \mathbb{N}$. Reproduction is only carried out by adults, while juveniles originate from this reproduction and some

metamorphose into adults in the next generation. The dynamics of the system are formulated as

$$\begin{cases} J_{t+1} = RA_t \exp\big(-aA_t^{\theta} - cJ_t^{\theta_J}\big), \\ A_{t+1} = \sigma A_t + sJ_t, \end{cases} \tag{1}$$

with parameters $R, a, c > 0$, $0 < s, \sigma < 1$, and $\theta, \theta_J > 0$.

Parameter R represents the maximum reproduction rate at low density, while a measures the strength of intraspecific competition among adults. Parameter c captures the feedback effect of juvenile density on the productivity of the next generation, which can be interpreted as ecological pressure due to the density of offspring or larvae on the same resource. Two exponents, θ and θ_J regulate the form of density nonlinearity for each stage; both allow for greater flexibility than the classic Ricker model, which has only one exponent. The proportion of juveniles that successfully reach adulthood is denoted by s, and σ indicates the probability of adult individuals surviving to the next generation.

When $c = 0$ and $\sigma = 0$, system (1) reduces to the standard two-stage Hassell–Ricker model without an intergenerational memory. If only the adult population is considered, the map shrinks to a one-dimensional Hassell form. Therefore, model (1) can be viewed as a generalization that combines stage structure effects, demographic memory, and density nonlinearity within a unified framework. Thus, the model remains compatible with the classical literature while providing additional degrees of freedom to accommodate inter-stage feedback effects.

2.2 Well-posedness and Boundedness (Basic Qualitative Properties)

Before analyzing the stability and bifurcation, it is important to ensure that system (1) has fundamental properties that guarantee the biological meaning of each trajectory. Two fundamental properties are required: positivity and boundedness. Positivity guarantees that the population density never takes on negative values, while boundedness ensures that the population does not grow indefinitely due to nonlinear imbalances. We demonstrate both properties below.

Lemma 1 (Positivity and forward invariance)**.** For every parameter $R, a, c > 0$, $0 < s, \sigma < 1$, and $\theta, \theta_J > 0$, if $(J_0, A_0) \in \mathbb{R}^2_{\geq 0}$, then the trajectory (J_t, A_t) generated by system (1) satisfies $(J_t, A_t) \in \mathbb{R}^2_{\geq 0}$ for all $t \geq 0$.

Proof. From the definition of a system (1), exponential function $\exp(-aA_t^{\theta} - cJ_t^{\theta_J})$ always positive for all $A_t, J_t \in \mathbb{R}_{\geq 0}$. Since $R > 0$ and $A_t \geq 0$, then

$$J_{t+1} = RA_t \exp(-aA_t^{\theta} - cJ_t^{\theta_J}) \geq 0.$$

In addition, with $s, \sigma \geq 0$, applicable

$$A_{t+1} = \sigma A_t + sJ_t \geq 0.$$

Since the right-hand side of each equation is nonnegative for $A_t, J_t \geq 0$, induction on t guarantees that if $(J_0, A_0) \in \mathbb{R}^2_{\geq 0}$, then $(J_t, A_t) \in \mathbb{R}^2_{\geq 0}$ for all $t \geq 0$. □

Lemma 1 guarantees that the trajectories do not exit the biological domains. Next, we show that all these trajectories remain bounded and do not exhibit infinite growth.

Lemma 2 (Boundedness)**.** For every parameter $R, a, c > 0$, $0 < s, \sigma < 1$, and $\theta, \theta_J > 0$, and for every positive initial condition $(J_0, A_0) \in \mathbb{R}^2_{\geq 0}$, there exists a number $M > 0$ such that the trajectory (J_t, A_t) of the system (1) satisfies

$$0 \leq J_t \leq M, \qquad 0 \leq A_t \leq M,$$

for all sufficiently large t. Thus, system (1) is bounded on $\mathbb{R}^2_{\geq 0}$.

Proof. From the first equation of system (1), we obtain the upper bound

$$J_{t+1} = RA_t \exp(-aA_t^{\theta} - cJ_t^{\theta_J}) \leq RA_t \exp(-aA_t^{\theta}).$$

The function $f(x) = Rxe^{-ax^{\theta}}$ reaches its maximum at $x = (1/(a\theta))^{1/\theta}$ with

$$f_{\max} = R\big(a\theta e\big)^{-1/\theta}.$$

Then, for all $A_t \geq 0$, the following applies

$$J_{t+1} \leq C_1 := R(a\theta e)^{\frac{-1}{\theta}}.$$

From the second equation, we obtain

$$A_{t+1} = \sigma A_t + sJ_t \leq \sigma A_t + sC_1.$$

Since $0 < \sigma < 1$, then for every $A_0 \geq 0$, the following applies

$$A_t \leq \sigma^t A_0 + sC_1 \sum_{k=0}^{t-1} \sigma^k \leq A_0 + \frac{sC_1}{1-\sigma}.$$

As a result, all trajectories satisfy

$$A_t \leq C_2 := A_0 + \frac{sC_1}{1-\sigma}.$$

Substituting back into the first equation yields

$$J_{t+1} \leq RC_2 e^{-aC_2^{\theta}} =: C_3.$$

By defining $M = \max\{C_1, C_2, C_3\}$, we obtain $0 \leq J_t, A_t \leq M$ for every $t \geq 0$. Note that the constant M depends on the parameters and initial conditions and proves that all trajectories eventually enter a compact invariant set. □

The two results above ensure well-posedness on positive orthants and guarantee that the dynamics are controlled (bounded), so that the subsequent calculation of fixed points and stability analysis are valid in the biological domain.

2.3 Existence and Uniqueness of Equilibria

We analyze the fixed points directly on the system in (1). The trivial equilibrium $(J^*, A^*) = (0, 0)$ always exists. For positive equilibria, define the demographic ratio

$$\eta = \frac{1-\sigma}{s}, \qquad \text{so that} \qquad J^* = \eta\, A^*.$$

Substituting into the first equation yields

$$a(A^*)^{\theta} + c\,\eta^{\theta_J}(A^*)^{\theta_J} = \log\Big(\tfrac{Rs}{1-\sigma}\Big). \tag{2}$$

Define also the function

$$g(A) := aA^{\theta} + c\,\eta^{\theta_J} A^{\theta_J}, \qquad A \geq 0.$$

Theorem 3 (Positive equilibrium and persistence threshold)**.** *For $R, a, c > 0$, $0 < s, \sigma < 1$, and $\theta, \theta_J > 0$, system* (1) *has:*

(i) trivial equilibrium $(J^*, A^*) = (0, 0)$ for all parameters;

(ii) exactly one positive equilibrium $(J^*, A^*) \in \mathbb{R}^2_{>0}$ if and only if

$$Rs > 1 - \sigma,$$

with $A^* > 0$ being the only solution to (2)*, and $J^* = \eta A^*$.*

Proof. Since $\theta, \theta_J > 0$ and $a, c > 0$, the function g is continuous and differentiable on $(0, \infty)$ with

$$g'(A) = a\theta A^{\theta-1} + c\,\theta_J\,\eta^{\theta_J} A^{\theta_J - 1} > 0.$$

Consequently, g is strictly increasing on $A > 0$, satisfies $g(0) = 0$, and satisfies $\lim_{A\to\infty} g(A) = \infty$. Thus, g constructs a homeomorphism from $[0, \infty)$ to $[0, \infty)$.

For the necessary condition, if $(J^*, A^*) > 0$ satisfies (2), then the right-hand side must be positive, so that $\log(\frac{Rs}{1-\sigma}) > 0$ or equivalently $Rs > 1 - \sigma$.

For the sufficient condition, assume $Rs > 1 - \sigma$ and write $h := \log(\frac{Rs}{1-\sigma}) > 0$. Since $g(0) = 0 < h$ and $g(A) \to \infty$ as $A \to \infty$, the Intermediate Value Theorem provides a $A^* > 0$ with $g(A^*) = h$. The monotonicity of g guarantees the uniqueness of A^*, whereas $J^* = \eta A^*$ completes the unique positive equilibrium. □

Lemma 4 (Uniqueness)**.** If $Rs > 1 - \sigma$, then the positive equilibrium of system (1) is unique.

Proof. Because g is strictly increasing, equation (2) has exactly one solution, $A^* > 0$. The relation $J^* = \eta A^*$ then uniquely determines J^*. □

Theorem 5 (Biological comparative statics)**.** *Suppose $Rs > 1 - \sigma$ and $A^* > 0$ satisfy* (2)*. The following holds:*

1. *A^* increases with respect to R, s, and σ, but decreases with respect to a and c;*
2. *the demographic ratio remains $J^*/A^* = \eta$, with*

$$\frac{\partial}{\partial\sigma}\Big(\frac{J^*}{A^*}\Big) = -\frac{1}{s} < 0, \; \frac{\partial}{\partial s}\Big(\frac{J^*}{A^*}\Big) = -\frac{1-\sigma}{s^2} < 0.$$

Biologically, an increase in fecundity (R) or maturation success (s) increases A^*, whereas competition (a) and juvenile feedback (c) decrease it. Adult survival (σ) increases the proportion of adults because it decreases the juvenile fraction at equilibrium.

Proof. Write (2) as $\Phi(A; R, s, \sigma, a, c) = 0$, with

$$\Phi(A; R, s, \sigma, a, c) = g(A) - \log\Big(\tfrac{Rs}{1-\sigma}\Big),$$
$$g(A) = aA^{\theta} + c\,\eta^{\theta_J} A^{\theta_J}.$$

Since $g'(A^*) > 0$, the Implicit Function Theorem gives

$$\frac{\partial A^*}{\partial \xi} = -\frac{\partial_\xi \Phi}{\partial_A \Phi} = -\frac{\partial_\xi \Phi}{g'(A^*)}, \qquad \xi \in \{R, s, \sigma, a, c\}.$$

The sign of each derivative follows directly from $\partial_\xi \Phi$ and $g'(A^*) > 0$; the interpretation is done *ceteris paribus*. □

Remark 1 (Continuity and regularity)**.** *If $Rs > 1 - \sigma$, then A^* is continuously and real-analytically dependent on each parameter because $g'(A^*) > 0$ and Φ is analytic on (A, R, s, σ, a, c).*

The threshold $Rs > 1 - \sigma$ marks the transition between extinction and persistence in the population. In this domain, the system has a unique positive equilibrium that varies smoothly with the parameters and provides a strong basis for the local stability analysis in the next section.

2.4 Local Stability Analysis

Once the existence and uniqueness of positive equilibrium are guaranteed, the next step is to assess its local stability in the presence of small perturbations. This analysis is based on the eigenvalues of the Jacobian matrix of the system around a fixed point, which determines whether the perturbation decreases, remains constant, or grows oscillatively.

For the system (1), the Jacobian in the general state (J, A) is given by

$$\mathcal{J}(J,A) = \begin{pmatrix} -RAe^{-\Phi}c\theta_J J^{\theta_J-1} & Re^{-\Phi}\big(1-a\theta A^{\theta}\big) \\ s & \sigma \end{pmatrix}$$
$$\Phi = aA^{\theta} + cJ^{\theta_J}. \tag{3}$$

Trivial equilibrium stability

For the extinction equilibrium, the Jacobian is understood in the limiting sense; in particular, differentiability at $J = 0$ is standard for $\theta_J \geq 1$. Substituting $(J, A) = (0, 0)$ into (3) yields

$$\mathcal{J}(0,0) = \begin{pmatrix} 0 & R \\ s & \sigma \end{pmatrix}, \qquad \chi(\lambda) = \lambda^2 - \sigma\lambda - Rs.$$

The Schur–Cohn criterion for the quadratic polynomial $\lambda^2 - \sigma\lambda - Rs$ states that all roots lie inside the unit circle if and only if

$$\begin{cases} 1 - \sigma - Rs > 0, \\ 1 + \sigma - Rs > 0, \\ 1 + Rs > 0. \end{cases} \tag{4}$$

Theorem 6 (Stability of trivial equilibrium)**.** *The trivial equilibrium $(0, 0)$ is locally asymptotically stable if $Rs < 1 - \sigma$, unstable if $Rs > 1 - \sigma$, and non-hyperbolic if $Rs = 1 - \sigma$.*

Proof. In the biological domain, that is, $0 < \sigma < 1$, the most restrictive inequality in (4) is $1-\sigma-Rs > 0$, that is, $Rs < 1 - \sigma$. The condition $1 + Rs > 0$ holds automatically for $R, s > 0$, and $Rs < 1 - \sigma$ also ensures $1 + \sigma - Rs > 0$. If $Rs > 1 - \sigma$, then at least one root satisfies $|\lambda| > 1$, so $(0, 0)$ loses stability. The threshold $Rs = 1 - \sigma$ corresponds to the emergence of a positive equilibrium in Theorem 3. □

Positive equilibrium stability

For $(J^*, A^*) > 0$ satisfying the equilibrium identity

$$a(A^*)^{\theta} + c\,\eta^{\theta_J}(A^*)^{\theta_J} = \log\Big(\tfrac{Rs}{1-\sigma}\Big) \tag{5}$$

the Jacobian at the fixed point is obtained as

$$\mathcal{J}^* = \begin{pmatrix} j_{11}^* & j_{12}^* \\ s & \sigma \end{pmatrix},$$
$$\Phi^* = a(A^*)^{\theta} + c(J^*)^{\theta_J}, \tag{6}$$

with $j_{11}^* = -RA^*e^{-\Phi^*}c\theta_J(J^*)^{\theta_J-1}$ and $j_{12}^* = Re^{-\Phi^*}\big(1 - a\theta(A^*)^{\theta}\big)$.

Because $J^* = \eta A^*$, all components of the Jacobian can be expressed only through A^* and the biological parameters.

Theorem 7 (Trace and determinant)**.** *With the substitution $J^* = \eta A^*$ and Φ^* from* (6)*, the trace and determinant of the Jacobian at positive equilibrium are given by*

$$\operatorname{tr}\mathcal{J}^* = \sigma - Re^{-\Phi^*}c\theta_J\,\eta^{\theta_J-1}(A^*)^{\theta_J}, \tag{7}$$

$$\begin{aligned} \det\mathcal{J}^* &= \big(-RA^*e^{-\Phi^*}c\theta_J(J^*)^{\theta_J-1}\big)\,\sigma \\ &\quad - \big(Re^{-\Phi^*}(1-a\theta(A^*)^{\theta})\big)\,s \\ &= -\sigma Re^{-\Phi^*}c\theta_J\,\eta^{\theta_J-1}(A^*)^{\theta_J} \\ &\quad - sRe^{-\Phi^*}\big(1-a\theta(A^*)^{\theta}\big). \end{aligned} \tag{8}$$

Proof. From (6), $\operatorname{tr}\mathcal{J}^* = a_{11} + a_{22}$ and $\det\mathcal{J}^* = a_{11}\sigma - a_{12}s$ for the matrix $\left[\begin{smallmatrix} a_{11} & a_{12} \\ s & \sigma \end{smallmatrix}\right]$. Substitute $a_{11} = -RA^*e^{-\Phi^*}c\theta_J(J^*)^{\theta_J-1}$, $a_{12} = Re^{-\Phi^*}(1 - a\theta(A^*)^{\theta})$, then use $J^* = \eta A^*$ so that $A^*(J^*)^{\theta_J-1} = \eta^{\theta_J-1}(A^*)^{\theta_J}$. This yields (7)–(8). Note that $\det\mathcal{J}^*$ need not be positive; a negative sign may arise due to the inhibitory feedback contribution to the entry a_{11}. □

This substitution yields a closed-form expression that depends entirely on A^* and the biological parameters. The local stability conditions for positive equilibrium follow the Schur–Cohn criteria, which can be explicitly written as

$$\begin{cases} 1 - \operatorname{tr}\mathcal{J}^* + \det\mathcal{J}^* > 0, \\ 1 + \operatorname{tr}\mathcal{J}^* + \det\mathcal{J}^* > 0, \\ 1 - \det\mathcal{J}^* > 0. \end{cases} \tag{9}$$

Equivalently, this is the 2×2 Jury condition which ensures that all roots of the characteristic polynomial lie inside the unit circle.

Remark 2 (Simplification and interpretation)**.** *If $\theta = \theta_J = 1$, then the system reduces to a linear-fractional step Hassell model. In this case,*

$$\operatorname{tr}\mathcal{J}^* = \sigma - Re^{-\Phi^*}\,c\,A^*,$$

so that σ enters linearly in both the trace and the determinant. Changes in adult survival therefore shift the location of the stability boundaries in parameter space, consistently with the intuition that higher adult persistence modifies the strength of oscillatory dynamics.

3 Local Bifurcation Analysis

This analysis focuses on changes in the stability of the positive equilibrium (J^*, A^*) discussed in Section 2. By tracing the trace $\operatorname{tr}\mathcal{J}^*$ and determinant $\det\mathcal{J}^*$ of the Jacobian (6), we can determine when fixed points lose their stability through two main mechanisms of two-dimensional maps: *flip* bifurcation (Period–doubling) and *Neimark–Sacker* bifurcation (quasiperiodic). The entire analysis is based on the characteristic polynomial

$$\lambda^2 - \operatorname{tr}\mathcal{J}^*\,\lambda + \det\mathcal{J}^* = 0, \tag{10}$$

with $\operatorname{tr}\mathcal{J}^*$ and $\det\mathcal{J}^*$ as given by (7)–(8).

The Schur–Cohn criterion for this quadratic polynomial states that all roots lie within the unit circle if and only if (9) holds.

Instability occurs when one of the equality conditions in (9) is satisfied. These two boundary conditions form a local bifurcation curve in the parameter space.

Regularity of the bifurcation curve. Before deriving the explicit conditions, we must ensure that the boundary curve is analytically smooth so that it can be traced continuously in the parameter space.

Proposition 8 (Regularity of the bifurcation curve)**.** *Define the boundary function*

$$\begin{aligned} F_{\text{flip}}(\mu) &= 1 + \operatorname{tr}\mathcal{J}^*(\mu) + \det\mathcal{J}^*(\mu), \\ F_{\text{NS}}(\mu) &= \det\mathcal{J}^*(\mu) - 1, \end{aligned} \tag{11}$$

where μ denotes the parameter vector of the system.

If for $\mu = \mu_*$ we have

$$\begin{aligned} F_{\text{flip}}(\mu_*) = 0 \quad (\textit{resp. } F_{\text{NS}}(\mu_*) = 0), \\ \nabla_\mu F_{\text{flip}}(\mu_*) \neq 0 \quad (\textit{resp. } \nabla_\mu F_{\text{NS}}(\mu_*) \neq 0). \end{aligned}$$

Then, the set of levels $F_{\text{flip}} = 0$ (resp. $F_{\text{NS}} = 0$) is a C^1 class curve in the parameter space.

Its partial gradient satisfies the relation

$$\frac{d\mu_i}{d\mu_j}\Big|_{\text{flip}} = -\frac{\partial_{\mu_j} F_{\text{flip}}}{\partial_{\mu_i} F_{\text{flip}}}, \qquad \frac{d\mu_i}{d\mu_j}\Big|_{\text{NS}} = -\frac{\partial_{\mu_j} F_{\text{NS}}}{\partial_{\mu_i} F_{\text{NS}}}. \tag{12}$$

Proof. The functions $\operatorname{tr}\mathcal{J}^*(\mu)$ and $\det\mathcal{J}^*(\mu)$ are smooth with respect to μ because they depend on $A^*(\mu)$, which is implicitly determined by (2). Suppose $F(\mu)$ is one of F_{flip} or F_{NS}. If $\nabla_\mu F(\mu_*) \neq 0$, then the Implicit Function Theorem guarantees the existence of a smooth function $\mu_i = \mu_i(\mu_j)$ in the neighborhood of μ_* that satisfies $F(\mu_i, \mu_j) = 0$.

Total differentiation $F(\mu_i, \mu_j) = 0$ gives

$$\frac{d\mu_i}{d\mu_j} = -\frac{\partial_{\mu_j} F}{\partial_{\mu_i} F},$$

which yields relation (12). This shows that the locus $F(\mu) = 0$ is a C^1-class one-dimensional manifold in the parameter space. □

This proposition guarantees that every boundary condition in (9) forms a smooth curve that can be traced numerically or analytically. Next, we examine the two mechanisms of instability separately.

(a) Flip Bifurcation

The first transition occurs when one of the eigenvalues reaches $\lambda = -1$.

Theorem 9 (Flip Bifurcation Condition for the θ–Ricker model)**.** *For system* (1) *with Jacobian* (6)*, a* flip *bifurcation occurs at parameter $\mu = \mu_*$ if and only if*

$$1 + \operatorname{tr}\mathcal{J}^*(\mu_*) + \det\mathcal{J}^*(\mu_*) = 0, \tag{13}$$

where $\operatorname{tr}\mathcal{J}^*$ *and* $\det\mathcal{J}^*$ *are given by* (7)–(8)*.*

and satisfies the transversality condition

$$\frac{d}{d\mu}(1 + \operatorname{tr}\mathcal{J}^* + \det\mathcal{J}^*)\Big|_{\mu=\mu_*} \neq 0. \tag{14}$$

Proof. Substituting $\lambda = -1$ into (10) yields the condition (13) By inserting the explicit forms of $\operatorname{tr}\mathcal{J}^*$ and $\det\mathcal{J}^*$ from (7)–(8), we obtain expression (13). The nonzero derivative guarantees that the eigenvalues cross -1 transversally, triggering the emergence of a two-periodic orbit in the phase space. The classical two-dimensional bifurcation theorem (See, [16]) completes this claim. □

The above conditions ensure that the emergence of two-generation oscillations occurs generically and not as a result of parametric degeneration. The sign change in the function F_{flip} determines the stable side of the parameter.

Lemma 10 (Stability exchange around the flip curve)**.** Around the curve $F_{\text{flip}} = 0$, the side with $F_{\text{flip}} > 0$ satisfies (9) and is therefore stable. If $\frac{d}{d\mu}F_{\text{flip}}(\mu_*) \neq 0$, then when μ crosses this curve, the stability of the fixed point switches between being stable and unstable.

Proof. The Schur–Cohn criterion shows that changing the sign of $F_{\text{flip}} = 1 + \operatorname{tr}\mathcal{J}^* + \det\mathcal{J}^*$ changes the number of roots inside the unit circle. Transversality ensures that this change is nonzero, such that one eigenvalue crosses $\lambda = -1$, causing a stability exchange. □

Biologically, an increase in σ (adult survival) increases the probability that the system will cross the flip threshold, and strong intergenerational memory reinforces oscillations between the two density levels.

(b) Neimark–Sacker bifurcation. The second transition occurs when a pair of complex conjugate eigenvalues crosses the unit circle.

Theorem 11 (Neimark–Sacker condition for the θ-Ricker model)**.** *Suppose* (J^*, A^*) *is a positive equilibrium of system* (1)*. Neimark–Sacker bifurcation occurs at* $\mu = \mu_*$ *if and only if*

$$sRe^{-\Phi^*}\big(1 - a\theta(A^*)^\theta\big) + \sigma Re^{-\Phi^*} c\theta_J\, \eta^{\theta_J - 1}(A^*)^{\theta_J} = -1, \qquad (15)$$

with the transversality condition

$$\frac{d}{d\mu}\big(\det \mathcal{J}^* - 1\big)\Big|_{\mu=\mu_*} \neq 0, \qquad (16)$$

and the nonresonance assumption

$$|\operatorname{tr} \mathcal{J}^*| < 2, \qquad \operatorname{tr} \mathcal{J}^* \notin \{-1, 0, 1\}. \qquad (17)$$

Proof. From (10), the conjugate complex roots lie on the unit circle if $\det \mathcal{J}^* = 1$ and $|\operatorname{tr} \mathcal{J}^*| < 2$. Substitution of (8) yields the explicit condition (15). Nonzero derivatives in (16) guarantee transversal crossing, while the assumption in (17) eliminates 1:2, 1:3, and 1:4 resonances. The standard Neimark–Sacker result (See, [**?**]) guarantees the appearance of small invariant circles around fixed points. □

This condition separates the parameter domain into a stable side ($\det \mathcal{J}^* < 1$) and oscillatory side ($\det \mathcal{J}^* > 1$). To determine the branch direction, we used the following first Lyapunov coefficient:

Proposition 12 (First Lyapunov coefficient)**.** *Write the map* (1) *as* $F(J, A)$*. At positive equilibrium, define the third-order derivative* $D^k F$*. Take the complex eigenpair* (λ, q) *and adjoint covector* p *of* $\mathcal{J}^*$ *satisfying*

$$\mathcal{J}^* q = \lambda q,$$
$$(\mathcal{J}^*)^\top p = \bar{\lambda} p,$$
$$\langle p, q\rangle = 1, \qquad |\lambda| = 1,\ \lambda \neq \pm 1.$$

Define the bilinear and trilinear

$$B(u, v) = \frac{1}{2} D^2 F[u, v],$$
$$C(u, v, w) = \frac{1}{6} D^3 F[u, v, w].$$

The first Lyapunov coefficient is

$$L_1 = \Re\Bigg(\frac{e^{-i\varphi}}{2} \Big\langle p,\ C(q, q, \bar{q}) + 2B\big(q, (I - \mathcal{J}^*)^{-1} B(q, \bar{q})\big) + B\big(\bar{q}, (e^{2i\varphi} I - \mathcal{J}^*)^{-1} B(q, q)\big) \Bigg).$$

with $\lambda = e^{i\varphi}$*. If* $L_1 < 0$*, the bifurcation is supercritical (stable circle); if* $L_1 > 0$*, it is subcritical (unstable circle).*

Proof. This formula results from the complex normal form of a two-dimensional map around a non-degenerate fixed point. By developing $F(x) = \mathcal{J}^* x + \frac{1}{2} D^2 F[x, x] + \frac{1}{6} D^3 F[x, x, x] + \cdots$, then projecting in the q and p directions, we obtain the expression L_1 above (see [**?**]). The sign of the L_1 signal determines the direction of the invariant circular branch. □

The above results allow for a complete classification: negative values of L_1 indicate stable circles (supercritical), whereas positive values indicate unstable circles (subcritical).

Lemma 13 (Stability exchange around the NS curve)**.** Around the curve $F_{\text{NS}} = 0$, the side with $F_{\text{NS}} < 0$ satisfies (9) and is stable. If $\frac{d}{d\mu} F_{\text{NS}}(\mu_*) \neq 0$, then crossing this curve changes the stability of the fixed point to a positive value.

Proof. Because $F_{\text{NS}} = \det \mathcal{J}^* - 1$, changing the sign of F_{NS} changes the modulus of the complex conjugate eigenvalue from < 1 to > 1. Transversality guarantees that this shift is simple, resulting in stability exchange between the equilibrium and invariant circles. □

Remark 3 (Biological interpretation and linear-fractional case)**.** *Condition* (15) *depends on* $(R, s, a, c, \theta, \theta_J)$ *via* Φ^* *and is linear with respect to* σ*. Therefore, the position of the Neimark–Sacker curve is primarily controlled by the interaction between reproduction and density regulation, whereas* σ *only affects the orientation of stability after bifurcation occurs.*

For the case $\theta = \theta_J = 1$, $\operatorname{tr} \mathcal{J}^*$ is linear in σ and $\partial_\sigma(1 + \operatorname{tr} + \det) > 0$ for reasonable biological parameters; therefore, the flip curve rises with respect to σ. This phenomenon is consistent with the intuition that higher adult persistence strengthens the demographic memory and promotes the emergence of periodic or quasiperiodic oscillations.

4 Numerical Experiments and Visualization

This section presents the numerical verification and visual exploration of the analytical results presented in the previous section. The aim was to ensure that the analytical conditions predicting the emergence of the flip and Neimark–Sacker bifurcations were consistent with the transitions observed numerically. All numerical procedures

follow standard iteration-based diagnostics for discrete dynamical systems, including transient removal, orbit sampling, and Lyapunov-based classification [7, 8].

The basic parameters used are

$$R = 20, \quad a = 0.5, \quad c = 1,$$

$$s = 0.8, \quad \sigma = 0.5, \quad \theta = \theta_J = 1.5,$$

Unless otherwise specified. The iteration is run until $(N_{\text{tot}} = 2 \times 10^4)$; the initial (10^4) steps are ignored as transient, then the orbit (A_t) is mapped to detect qualitative changes due to parameter variations. Initial conditions are chosen in the positive quadrant, and the reported qualitative regimes were observed to be consistent under other biologically reasonable positive initial states.

This numerical analysis was divided into two parts: (i) a one-dimensional bifurcation diagram that traces the change in orbits against variations in a single parameter, and (ii) a two-dimensional map of the largest Lyapunov exponent that shows the global structure of the dynamic regime. For each parameter sweep, the same transient length and sampling window are used to maintain comparability across panels.

4.1 One-Dimensional Bifurcation

Previous analytical results (see Prop. 8) show that the conditions $F_{\text{flip}}(\mu) = 0$ and $F_{\text{NS}}(\mu) = 0$ mark the appearance of flip and Neimark–Sacker bifurcations. This section shows how these boundaries manifest numerically using a one-parameter bifurcation diagram.

The following figures show the transition of orbit A_t with respect to a single parameter variation, while the red curve presents the largest Lyapunov exponent (LLE) value. The change from one fixed point to two, four, and so on reflects a flip bifurcation, whereas the LLE crossing zero indicates a loss of stability or a transition to chaos. The LLE is computed using a standard Jacobian-product renormalization approach for discrete maps, implemented along the post-transient orbit to detect stability loss and chaotic windows in a consistent way [7].

In Figure 1, an increase in R indicates a typical logistic bifurcation chain. The fixed orbit loses stability through successive double-folds until a chaotic band appears. This phenomenon is consistent with the analytical result that a high value of R enlarges the diagonal elements of the Jacobian, causing tr $\mathcal{J}^*$ to exceed the stability boundary $(-1, 1)$ and triggering $F_{\text{flip}} = 0$.

When a decreases (Figure 2), the competitive pressure weakens, and stability decreases. Small values of a result in period doubling, leading to

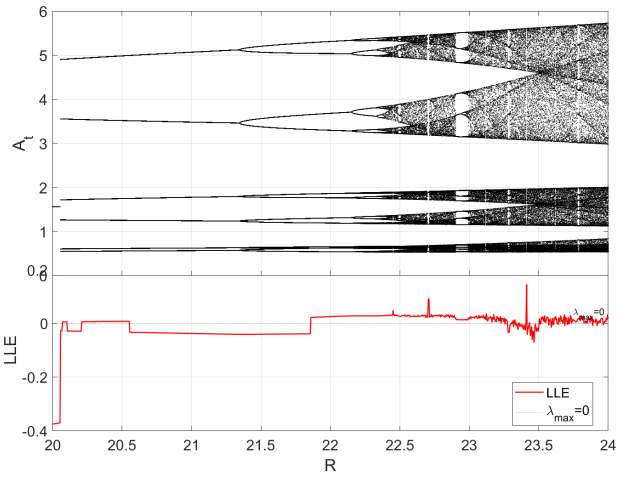

Figure 1: Bifurcation diagram against maximum fecundity R. (Source: created by the authors.)

chaos. Analytically, parameter a affects the position of fixed point A^* and the local gradient of the map. When a decreases, the negative contribution to $\partial_A F$ weakens, so that the eigenvalues become greater than -1, crossing the boundary $F_{\text{flip}} = 0$.

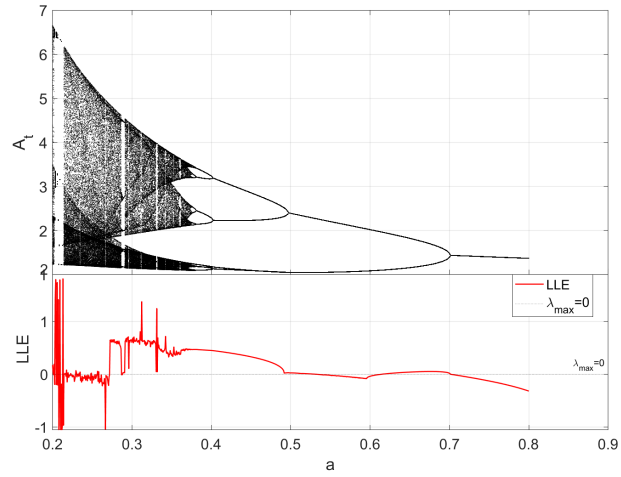

Figure 2: Bifurcation diagram against competition intensity a. (Source: created by the authors.)

An increase in c (Figure 3) strengthens the juvenile feedback effect on the recruitment. A cascade of bifurcations is observed around $c \approx 1.4$, followed by a periodic window and a wide chaotic band. This structure indicates that c not only affects local stability but also triggers nonlinear interactions between the two age stages, potentially causing Neimark–Sacker bifurcation in the parameter pair (R, c).

As shown in Figure 4, for $s < 0.1$, the orbit approaches zero, but when s increases past the threshold of ≈ 0.15, a stable fixed point appears and

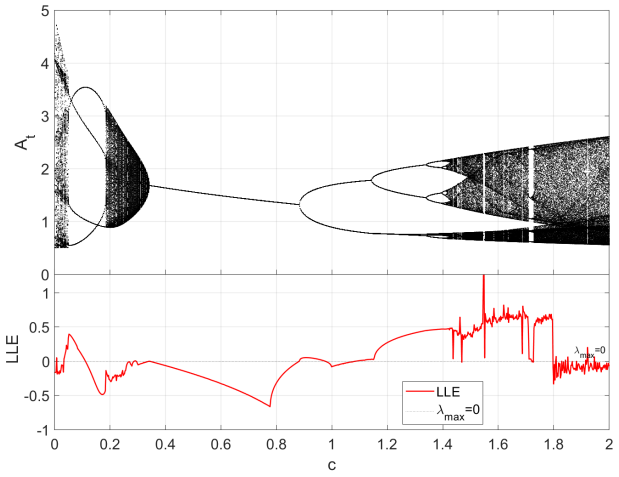

Figure 3: Bifurcation diagram for cross-stage coupling c. (Source: created by the authors.)

persists until $s \approx 0.6$. This stability correlates with the value $\det(\mathcal{J}^*) < 1$ which keeps the system in the Schur domain. The transition to small oscillations at $s \approx 0.65$ marks the proximity to the boundary $F_{\text{NS}} = 0$.

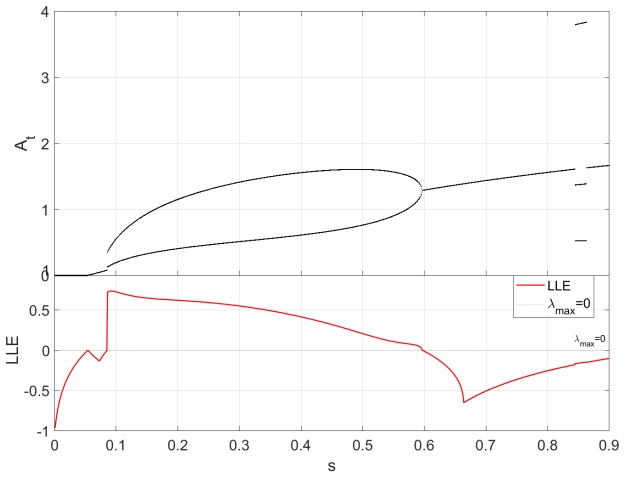

Figure 4: Bifurcation diagram against maturation success s. (Source: created by the authors.)

Variations in σ (Figure 5) show the effects of demographic memory. For small σ, a cascade of double folds appears, while an increase in σ compacts the branches until the orbit returns to a stable state. This reinforces the analysis that the memory parameter plays a role in keeping the orbit within the stability domain by decreasing $\operatorname{tr} \mathcal{J}^*$. In other words, an increase in σ increases internal damping of the system.

An increase in θ (Figure 6) causes instability at a certain threshold and indicates a quasiperiodic

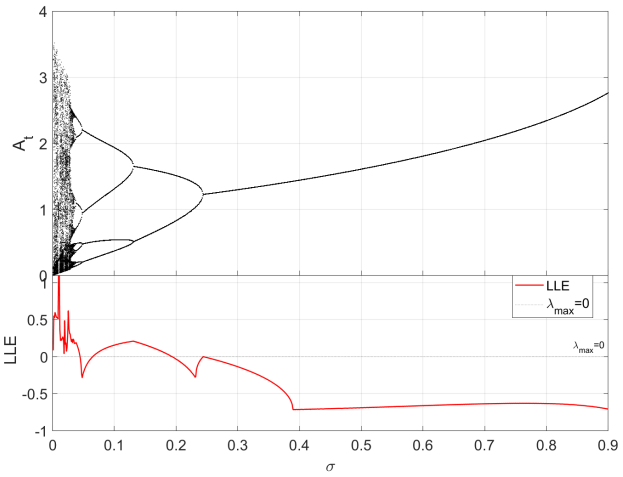

Figure 5: Bifurcation diagram for adult survival σ. (Source: created by the authors.)

state. For $\theta > 1.7$, the LLE shows small positive oscillations, indicating a smooth transition to quasiperiodicity, consistent with the condition $F_{\text{NS}}(\mu) = 0$. This indicates that the Neimark–Sacker bifurcation occurs on this path, as predicted by the local analysis.

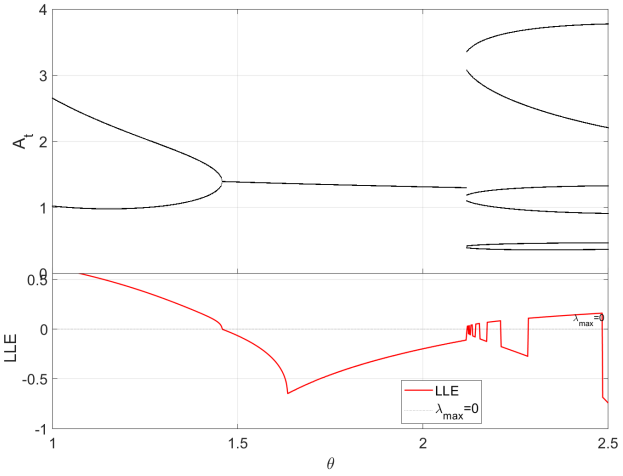

Figure 6: Bifurcation diagram against the adult density exponent θ. (Source: created by the authors.)

Figure 7 shows a period–doubling cascades under variations of θ_J, similar to the θ case but sharper. When $\theta_J > 1.3$, the system experiences a rapid bifurcation cascade towards chaos. Juvenile dominance in the recruitment function causes high sensitivity to small changes in parameters. Analytically, this is reflected in the increase in $\partial_\mu F_{\text{flip}}$, which indicates a sharp bifurcation curve gradient, as in Prop. 8.

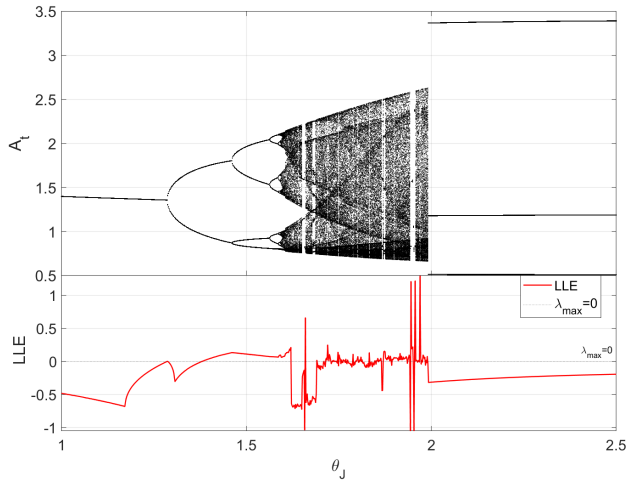

Figure 7: Bifurcation diagram for juvenile density exponent θ_J. (Source: created by the authors.)

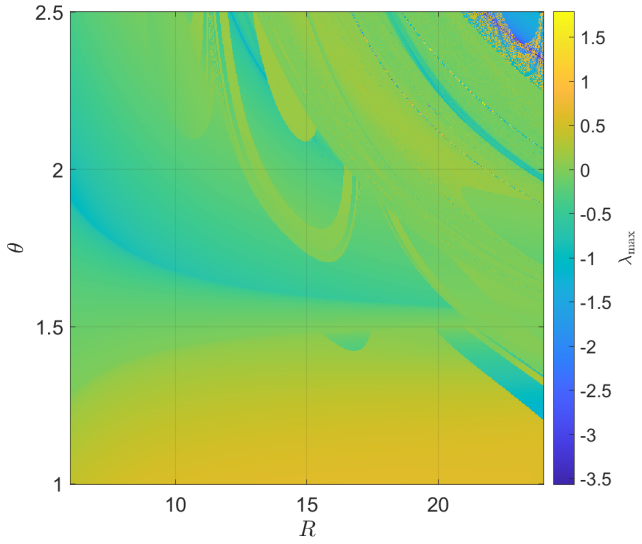

Figure 8: Map of $\lambda_{\max}$ on the plane (R, θ). (Source: created by the authors.)

4.2 Two-Dimensional Parameter Map

After exploring the dynamics of a single parameter, the analysis continues with the exploration of two parameters to identify the global structure in the space $\mu = (R, \theta, c, s, \sigma)$. The following maps display the largest Lyapunov exponent $\lambda_{\max}$ as a function of two parameters, illustrating how the domains of stability and chaos interact. The two-parameter scans are computed on a uniform grid in each plane, using the same transient removal and LLE evaluation protocol as in the one-parameter diagrams to ensure coherent regime classification.

In Figure 8, the chaotic tongues appear in tiers around $\theta \approx 2$. The stable blue zone ($\lambda_{\max} < 0$) dominates for $\theta < 1.5$, but begins to break up into narrow windows of chaos as θ increases. This result confirms that an increase in the adult density exponent accelerates the loss of stability, as indicated by the analytical condition $F_{\text{NS}} = 0$.

Figure 9 shows a branched structure with chaos bands at $c > 1.2$ and a stable blue window below it. This phenomenon indicates that the strengthening of cross-stage feedback expands the unstable region that is nonlinear with respect to R. Qualitatively, this shape is similar to a two-dimensional fold described by the gradient relation (12).

In Figure 10, an increase in s expands the stable blue area, indicating a damping effect on the oscillations. For $s > 0.6$, no chaotic zones were found. These results are consistent with one-dimensional observations that maturation efficiency acts as a neutralizing factor in the dynamics.

Figure 11 confirms the memory effect: the large yellow-chaos zone at $\sigma < 0.4$ gradually narrows and disappears when $\sigma > 0.6$. The gentle vertical color gradient illustrates the role of σ as a mechanism for damping dynamic transitions. This finding reinforces the theoretical result that increasing σ keeps the eigenvalues within the unit disk.

Numerical and analytical results are consistent. The boundary ($F_{\text{flip}} = 0$) marks a double fold in the variation (R, a, c), while ($F_{\text{NS}} = 0$) triggers a quasiperiodic transition in (θ, θ_J, s). The two-parameter map highlights the interactions of reproduction, cross-stage coupling, maturation, and memory that determine the direction and rate of chaos. This system has two main paths to chaos, namely bifurcation cascades and Neimark–Sacker bifurcations that produce unstable tori, both of which are consistent with the previous analytical framework.

5 Ecological Implications and Discussion

After obtaining analytical and numerical results, attention is directed to ecological significance, namely how biological mechanisms shape the direction of population dynamics evolution. Two main mechanisms, demographic memory through adult survival σ and cross-stage feedback c, regulate stability by influencing the trace and determinant of the Jacobian matrix at positive fixed points so that changes in stability are determined by the flip boundaries $F_{\text{flip}} = 0$ and Neimark–sacker boundaries $F_{\text{NS}} = 0$.

The parameter σ acts as a stabilizer. An increase in σ increases intergenerational survival, stabilizes fixed orbits, and decreases the largest Lyapunov exponent to a negative value on the map (R, σ); ecologically,

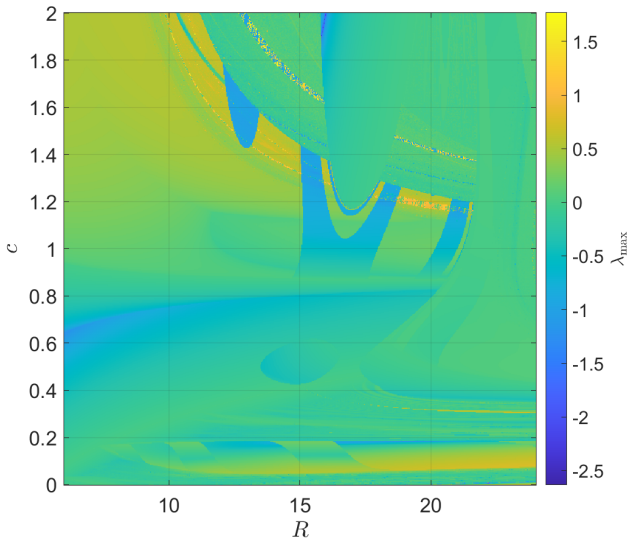

Figure 9: Map of $\lambda_{\max}$ in the (R, c) plane. (Source: created by the authors.)

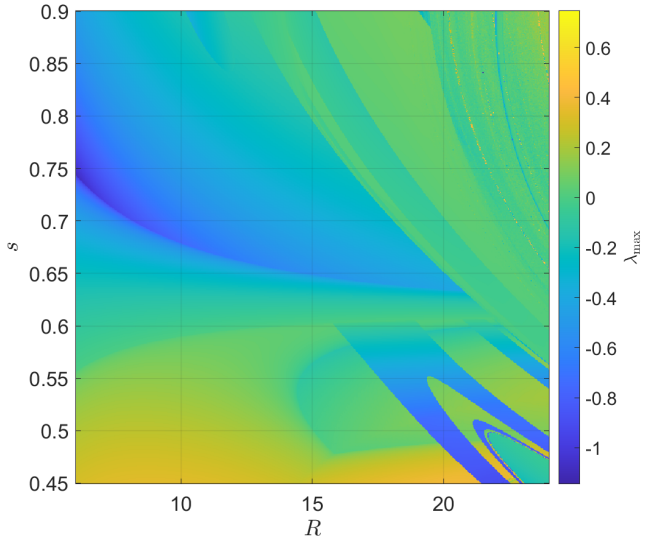

Figure 10: Map of $\lambda_{\max}$ in the (R, s) plane. (Source: created by the authors.)

this dampens density oscillations and delays the transition to chaos. Conversely, reproduction R and competition among adults a promote instability: an increase in R triggers a bifurcation cascade (Figure 1), while a decrease in a weakens regulation and accelerates the emergence of oscillations. Both modify the linear component $\mathcal{J}^*$ and the boundary $F_{\text{flip}} = 0$.

Cross-stage coupling c strengthens juvenile–adult linkage by altering the nondiagonal elements of the Jacobian, increasing the system's sensitivity to parameter changes to produce recurrent bifurcation patterns leading to chaotic behavior; an increase in c can shift the system out of the stable domain even if other parameters remain constant. The maturation parameter s maintains stability, as an increase in s accelerates convergence to a positive fixed point and widens the range with $\lambda_{\max} < 0$, which ecologically reflects the accelerated recovery of the adult class, thereby resisting fluctuations.

The density exponents θ and θ_J regulate the strength of the population's response to the density at each stage. The numerical results show that an increase in both parameters leads to the emergence of recurrent bifurcation patterns and narrow stability windows. Mathematically, this is related to changes in the shape of the growth function at fixed points, which affect the local derivative value $D_A F$ and ultimately the stability of fixed orbits.

Overall, the analytical and numerical results are consistent. Parameters that increase the Jacobian trace value, such as R, a, and c, tend to push the system past the stability boundary $F_{\text{flip}} = 0$ and produce oscillatory or chaotic dynamics. Conversely, parameters that decrease the trace value, such as σ and s, expand the stability domain and keep the orbit convergent. These findings provide a quantitative explanation for the role of biological mechanisms in regulating the stability of stage-structured population.

From an ecological perspective, the results confirm that adult survival and maturation success serve as natural buffers against population fluctuations, whereas high productivity and strong cross-stage interactions can induce instability. Thus, conservation strategies that focus on increasing adult survival or maturation efficiency have the potential to expand the population stability domain. Conversely, pest or invasive species control can be achieved by reducing adult survival or strengthening inter-stage feedback effects to accelerate instability and population decline. These results show that stage-structured mathematical models not only explain population dynamics theoretically but also provide a quantitative framework for designing more adaptive and predictive ecosystem management policies.

6 Conclusion

This study developed a two-stage θ-Ricker map-based population model that incorporates demographic memory effects through adult survival (σ). This formulation extends the classic Hassell model by adding an intergenerational survival mechanism, such that the behavior of the system is determined not only by the reproduction rate but also by the cross-stage interaction between juveniles and adults. This approach provides a more realistic mathematical framework for understanding

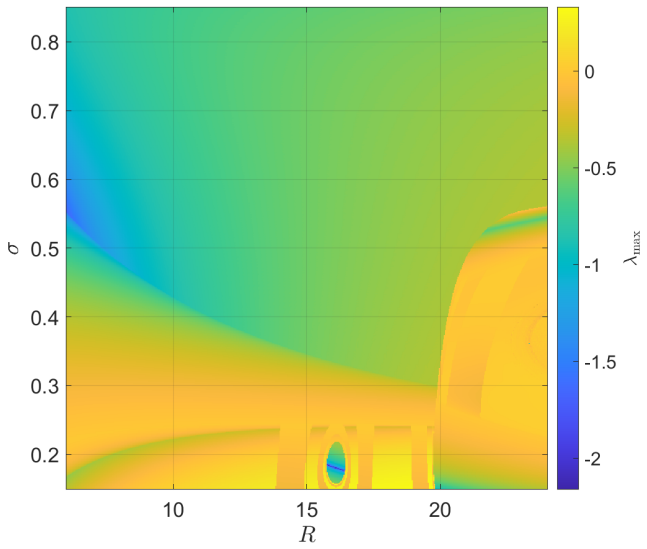

Figure 11: Map of $\lambda_{\max}$ in the (R, σ) plane. (Source: created by the authors.)

the dynamics of stage-structured populations both analytically and numerically.

Theoretical analysis shows that the system has a unique positive equilibrium when the condition $Rs > 1 - \sigma$ is satisfied. The stability of this equilibrium depends on the trace value and determinant of the Jacobian matrix at the fixed point, with two main mechanisms of instability: flip bifurcation and Neimark–Sacker bifurcation. The boundary $F_{\text{flip}}(\mu) = 0$ marks the emergence of a two-periodic orbit, whereas the condition $\det \mathcal{J}^* = 1$ indicates a transition to quasiperiodic oscillations. Further analysis via the first Lyapunov coefficient confirms that the direction and type of bifurcation are determined by the sign of L_1, which separates the supercritical (stable circle) and subcritical (unstable circles) cases.

The numerical results reinforce these analytical findings. The one-dimensional bifurcation diagram shows that an increase in the reproductive parameter (R) or strengthening of cross-stage feedback (c) drives the system towards repeated doubling until chaos, whereas an increase in adult survival (σ) and maturation rate (s) expands the region of stability. A two-dimensional map of the Lyapunov exponents shows the transition domain between stable, quasiperiodic, and chaotic orbits in line with the locally derived bifurcation curve. The consistency between the theoretical analysis and numerical simulation indicates that the stage structure and demographic memory quantitatively control the direction of the system dynamics.

Ecologically, these results highlight that adult survival and maturation success serve as natural buffers against population fluctuations, whereas increased productivity or excessive cross-stage interactions can lead to instability. Thus, this model not only explains the mathematical mechanisms behind the emergence of bifurcation and chaos in stage-structured systems but also offers insights into population management: strengthening adult survival and juvenile–adult transition efficiency can maintain population stability, while extreme parameter combinations have the potential to trigger irregular dynamics. This conclusion reinforces the idea that the integration of stage structure, cross-stage feedback, and demographic memory is key to understanding and predicting the complexity of population dynamics in real ecosystems.

Acknowledgment:
The author would like to express sincere gratitude to Universitas Diponegoro for the financial support provided through the Non-State Budget Funding Scheme (Dana selain APBN) for Fiscal Year 2025, based on the Decree of the Head of the Institute for Research and Community Service of Universitas Diponegoro (LPPM), No. 610/UN7.D2/HK/III/2025, dated March 18, 2025, and the Contract Agreement Number: 222-179/UN7.D2/PP /IV/2025 dated April 8, 2025.

References:

[1] El–Metwally, H., Alsulami, I. M., & Hamada, M. Y. (2024). On a generalized discrete Ricker map. *AIMS Mathematics*, *9*(14), 41417. https://doi.org/10.3934/math.20241417.

[2] H. A. El-Morshedy and A. Ruiz-Herrera. Attraction to equilibria in discrete population models with delayed feedbacks: stage-structure versus age-structure. *Journal of Mathematical Biology* **90** (2025), 40. doi: https://doi.org/10.1007/s00285-025-02200-5.

[3] M. M. Khan and M. J. Uddin. Chaos and bifurcations of a discretized Holling-II prey–predator model including prey refuge and Allee effect. *Scientific Reports* **15** (2025), 32940. doi: https://doi.org/10.1038/s41598-025-04333-5.

[4] K. Mokni, M. Ch-Chaoui. Exploring persistence, stability, and bifurcations: a Darwinian Ricker–Cushing model. *International Journal of Dynamics and Control* **13** (2025), 34. doi: https://doi.org/10.1007/s40435-024-01539-9.

[5] G. Papaschinopoulos, C. J. Schinas, G. Ellina. On the dynamics of the solutions of a biological

model. *Journal of Difference Equations and Applications* **20**(5–6) (2014), 694–705. doi: https://doi.org/10.1080/10236198.2013.806493.

[6] G. Papaschinopoulos, N. Fotiades, C. J. Schinas. On a system of difference equations including negative exponential terms. *Journal of Difference Equations and Applications* **20**(5–6) (2014), 717–732. doi: https://doi.org/10.1080/10236198.2013.814647.

[7] S. N. Elaydi. *An Introduction to Difference Equations*, 3rd ed. Undergraduate Texts in Mathematics. Springer, New York, 2005. doi: https://doi.org/10.1007/0-387-27602-5. ISBN-10: 0387230599; ISBN-13: 978-0387230597.

[8] R. M. May. Simple mathematical models with very complicated dynamics. *Nature* **261** (1976), 459–467. doi: https://doi.org/10.1038/261459a0.

[9] E. Liz and P. Pilarczyk. Global dynamics in a stage-structured discrete-time population model with harvesting. *Journal of Theoretical Biology* **297** (2012), 148–165. doi: https://doi.org/10.1016/j.jtbi.2011.12.012.

[10] H. Mo and Y. Shao. Stability and bifurcation analysis of a delayed stage-structured predator–prey model with fear, additional food, and cooperative behavior in both species. *Advances in Continuous and Discrete Models* **2025** (2025), 27. doi: https://doi.org/10.1186/s13662-025-03879-y.

[11] Y. Liu, L. Guo, X. Liu. Dynamical Behaviors in a Stage-Structured Model with a Birth Pulse. *Mathematics* **11** (2023), 3321. doi: https://doi.org/10.3390/math11153321.

[12] Y. Song and Y. Peng. Stability and bifurcation analysis on a logistic model with discrete and distributed delays. *Applied Mathematics and Computation* **181** (2006), 1745–1757. doi: https://doi.org/10.1016/j.amc.2006.03.025.

[13] E. Liz and E. Sovrano. Stability, bifurcations and hydra effects in a stage-structured population model with threshold harvesting. *Communications in Nonlinear Science and Numerical Simulation* **109** (2022), 106280. doi: https://doi.org/10.1016/j.cnsns.2022.106280.

[14] V. S. Sharma, A. Singh, A. Elsonbaty, A. A. Elsadany. Codimension-one and -two bifurcation analysis of a discrete-time prey–predator model. *International Journal of Dynamics and Control* **11**(6) (2023), 2691–2705. doi: https://doi.org/10.1007/s40435-023-01177-7.

[15] M. O. Al-Kaff, H. A. El-Metwally, A.-E. A. Elsadany, E. M. Elabbasy. Exploring chaos and bifurcation in a discrete prey–predator based on coupled logistic map. *Scientific Reports* **14** (2024), 16118. doi: https://doi.org/10.1038/s41598-024-62439-8.

[16] Y. A. Kuznetsov. *Elements of Applied Bifurcation Theory*, 3rd ed. Springer, 2004. doi: https://doi.org/10.1007/978-1-4757-3978-7.

Contribution of Individual Authors to the Creation of a Scientific Article (Ghostwriting Policy)

H.K.F. discussed the results, analyzed the model, wrote, and reviewed the manuscript. N.Y.A. supervised the study, wrote, performed numerical simulations, and reviewed. All authors read and approved the final version.

Conflicts of Interest

The authors have no conflicts of interest to declare that are relevant to the content of this article.

Compliance Statement

The authors confirm that this manuscript does not duplicate material from prior publications. Any reused background content is properly cited, and the present work is original in its analysis, formulation, and numerical evidence.

Creative Commons Attribution License 4.0 (Attribution 4.0 International , CC BY 4.0)

This article is published under the terms of the Creative Commons Attribution License 4.0
https://creativecommons.org/licenses/by/4.0/deed.en_US